THE ASTROPHYSICAL JOURNAL, 255:329–340, 1982 April 1

CHARGE ABUNDANCE OF COSMIC RAYS AT THEIR SOURCE

W. R. WEBBER
Space Science Center, University of New Hampshire
Received 1981 August 3; accepted 1981 October 7

ABSTRACT

The relative charge abundance of galactic cosmic-ray nuclei has been measured between 600 and 1000 MeV per nucleon over a range of Z from 2 to 28. The abundances observed at Earth have been extrapolated to the cosmic-ray source yielding accurate source abundances for 15 elements. These abundances, along with recently measured isotopic abundance ratios, are compared with the average abundances observed in another sample of accelerated material—solar cosmic rays. Significant differences are found in the composition for the elements He, C, N, and Ne. These galactic and solar cosmic-ray abundances are also compared with a variety of compilations of unaccelerated matter. This comparison is complicated by normalization problems for the O/Si ratio and by uncertainties in the normalization procedures used to obtain the He, Ne, and Ar abundances in these abundance compilations. In view of these difficulties, we have examined more carefully the very clear differences between the two accelerated species. At the present time, these differences seem to be explained more easily in terms of differing nucleosynthesis histories rather than preferential acceleration effects.

The new galactic cosmic-ray source charge ratios presented here along with specific isotopic abundance differences that are observed require new calculations in the areas of both nucleosynthesis theory and preferential acceleration and present a new challenge to the attempt to locate the source regions of galactic cosmic rays.

Subject headings: cosmic rays: abundances — particle acceleration

I. INTRODUCTION

Recently, it has become possible to obtain the source abundances of galactic cosmic-ray nuclei with much improved accuracy. The precision of solar cosmic-ray abundance data has also improved dramatically in the last few years, and it has been shown that, for energies above a few MeV per nucleon, these solar cosmic-ray abundances provide meaningful and accurate average abundance ratios when many events are summed. It seems natural then to compare the abundances of these two species since they both represent samples of matter accelerated to high energies. From such a comparison and the differences observed, one might hope to identify differences between the two acceleration processes or differences between the nucleosynthesis histories of the two classes of particles.

Comparisons of cosmic-ray abundances with universal abundances or solar system abundances have been made for many years. When such comparisons are made, it is found that cosmic rays with the lowest first ionization potential are overabundant relative to solar system material. This correlation with first ionization potential has been established in several studies and has recently been found to extend to the trans-iron nuclei abundances (Binns *et al.* 1981). This has been interpreted by many authors to indicate a preferential acceleration effect in the cosmic-ray sources (Kristiansson 1971; Havnes 1973; Cassé and Goret 1978). But it has also been noted that the solar cosmic-ray abundances, when compared with the solar system abundance data, show a similar but not precisely identical correlation with first ionization potential (Webber 1975). Is this also indicative of a similar preferential acceleration effect for solar cosmic rays? It is well known that there are large differences in various solar abundance determinations—particularly between the photospheric and coronal abundances. Could it be that comparisons of the abundances of accelerated cosmic rays with general solar system abundances are inappropriate for actually determining possible preferential acceleration effects or differences in the underlying composition in the specific cosmic-ray acceleration regions?

In an endeavor to place this important question in a new perspective, we have derived, based on a balloon experiment, a new set of more precise cosmic-ray source abundances for 15 elements ranging from He to Ni. This analysis uses the same data base as in recently reported isotopic composition measurements (Webber 1982) but emphasizes and extends the charge composition aspect of the data. The new abundance measurements are compared with the solar cosmic-ray composition measurements as well as a variety of abundance compilations for unaccelerated matter including solar photospheric and coronal data.

II. THE INSTRUMENT AND ITS OPERATION

The telescope used in these measurements has been discussed in several earlier publications (Lezniak and Webber 1978, hereafter LW; Webber 1982.) The results

reported here represent the combined data from two balloon flights made with this telescope under "quiet" sunspot minimum modulation conditions in 1976 September and 1977 September. The average residual atmospheric depth of the two flights was 3.3 g cm^{-2}, and the combined useful exposure factor was 23,300 cm^2 sr^{-1} s^{-1}. This provides data of a high statistical accuracy. An outline drawing of the telescope is shown in Figure 1. The telescope contains two modules: the upper module contains a combination of scintillation and Cerenkov counters to measure the charge and energy of the particles; the lower module contains four thick, total energy scintillators which are used to measure the total energy of low-energy particles to determine their mass using the Cerenkov x total energy technique. Each of the individual counters were contained in white diffusion boxes whose uniformity was measured to $\sim 1\%$ FWHM by a ^{207}Bi electron source.

In this paper, we are concerned only with the charge and energy spectrum measurements made in the first module. A basic telescope event occurs when a coincidence is made between the scintillators S1 and S2. Two trigger levels are employed, one at 6 times the minimum ionization for a $Z = 1$ particle, thus counting all nuclei with $Z \geq 3$ with full efficiency, and another trigger level at 0.5 times the minimum ionizing to count the much more abundant proton and helium nuclei with a scaling factor of 16. Master tapes of the flight data, corrected for small gain variations and path length variations, were constructed. These tapes were used to construct the multidimensional matrices used for data analysis.

III. DATA ANALYSIS PROCEDURES

The initial goal of the data analysis is to obtain a class of events that represent single particle traversals of the telescope without interaction. Events due to particles,

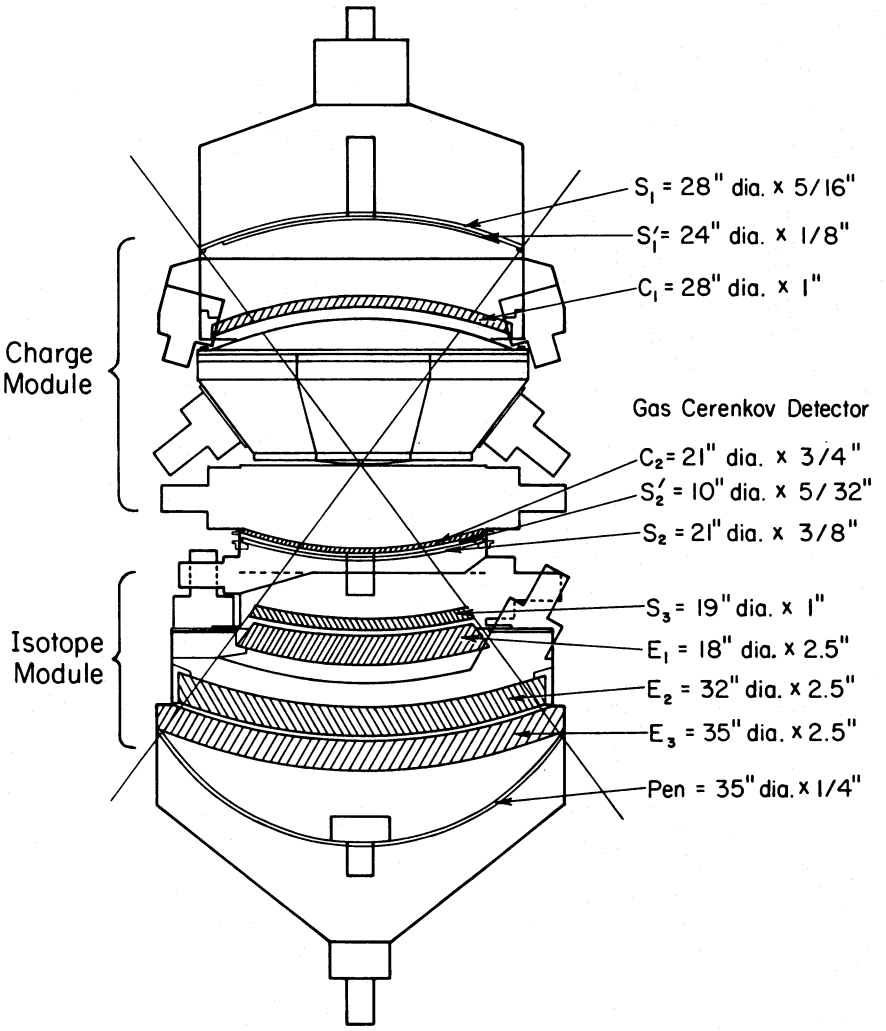

FIG. 1.—Outline drawing of cosmic-ray charge-isotope telescope

either within the telescope geometry or outside it, that interact in the telescope and other types of background events must be identified and removed without introducing a charge or energy bias. The procedures used to accomplish this have been discussed in LW. Identical analysis procedures are followed throughout for both balloon flights. We have used a simple consistency criterion on the S1 and S2 counter outputs of the form

$$\frac{2|\mathrm{S1}-\mathrm{S2}|}{\mathrm{S1}+\mathrm{S2}} < X\rho\ ,$$

where ρ is a function that is proportional to the resolution of the S1 and S2 counters and X is a variable parameter. The width of the selection band may be changed by varying X to study the effects on both the background and the desired events on the matrices under study. Optimum rejection of background is achieved when X is chosen so that the selection passband is $\sim 3\ \sigma$ for all charges where σ is the observed rms resolution of the S1 and S2 counters as determined from the pulse height distributions of the individual charges. This criterion is found to eliminate $\leq 2\%$ of the desired events, and this fraction is verified to be essentially charge and energy independent. The identification of interacting nuclei and other background events is determined to be $90 \pm 5\%$ efficient. New data tapes that are prepared using this criteria have $\sim 60\%$ as many counts as the original tapes. Desired multidimensional matrices may be made directly from these tapes. An example of such a matrix (S1 + S2)/2 versus C2 is shown in Figure 3 of LW. Matrices like the one above may be used to obtain the charge composition and energy spectrum of incident particles. The charge separation on these matrices is excellent; for example, the charge F adjacent to O and with an abundance $\sim 1\%$ of O can be seen clearly. A charge histogram of events used in this analysis is shown in Figure 2. The charge resolution σ varies from 0.08 charge units at C, to 0.14 charge units at Si, to 0.22 charge units at Fe.

If one constructs a matrix of events with (S1 + S2)/2 versus C2 as above, then events will lie along lines defined by the relationships

$$S = K_s \frac{Z^2}{\beta^2} f(Z, \beta) \quad \text{and} \quad C = K_c Z^2 \left(1 - \frac{\beta_0^2}{\beta^2}\right).$$

Each charge will be represented by a particular line in S versus C space, and the various energies will be located at various points along this line. Essentially the energy spectrum is unfolded in C space. For each separately identified charge, a distribution of events along the charge line in the C dimension may be obtained. Examples of such Cerenkov distributions for several nuclei are shown in Figure 3. The procedures for unfolding the energy spectrum of a particular charge from such a pulse height distribution has been discussed in detail by LW. Here, we use a very simplified application of these procedures since we are interested in determining the relative intensity of various charges in a single common energy interval from 600 to 1000 MeV per nucleon at the top of the atmosphere. This interval is chosen because the most accurate cross section measurements are available at these energies, allowing for a better extrapolation to the sources, and also because effects that complicate interpretation of the low-energy abundance data (e.g., solar modulation and uncertain galactic propagation path length) are minimized. This data will be the basis of our charge composition comparisons.

Consider Figure 3 which shows the Cerenkov distributions for several nuclei. The energy scale is completely determined when $C_{\max}$ is located, e.g.,

$$C = C_{\max} \frac{1 - \beta_0^2/\beta^2}{\beta_0^2},$$

where β_0 is the threshold velocity. The location of $C_{\max}$ from the pulse height distribution is obtained using the procedures discussed by Lezniak (1975). The location of the various energies in terms of $C_{\max}$ is shown in Figure 3 and in Table 1. The band from 600 to 1000 MeV per nucleon is shown as a shaded area in Figure 3. The number of events that fall into this energy bin is $N_m(\Delta E)$. The relationship between this quantity and the true number of

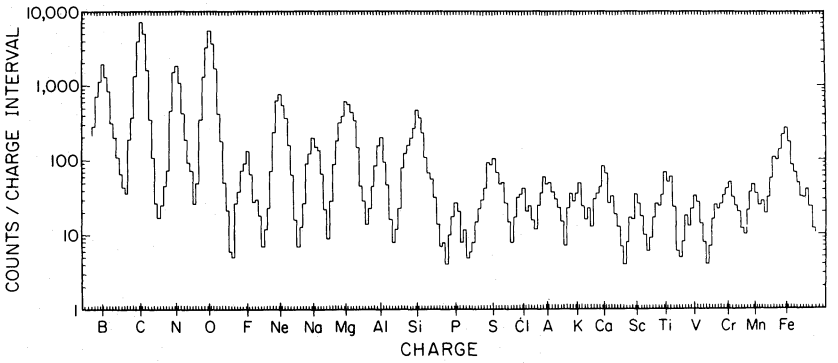

FIG. 2.—Charge histogram of events in 600–1000 MeV per nucleon energy range

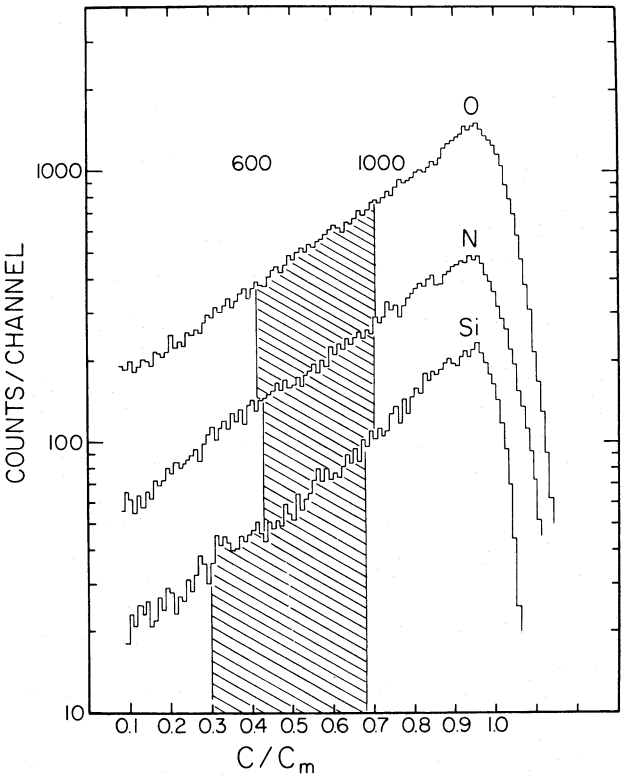

FIG. 3.—Cerenkov distributions for O, N, and Si nuclei. Energy band from 600 to 1000 MeV per nucleon shown as shaded region.

events may be written $N(\Delta E) = N_m(\Delta E) \times F$, where F is a correction factor depending on (1) the energy interval, (2) the Cerenkov resolution, and (3) the energy spectrum. If the instrumental resolution is much less than the interval width ΔE, then $F \sim 1$ and the correction is independent of the spectrum. This is the case for the energy interval and charges involved in this analysis.

Once the number of events N has been determined, it is further necessary to correct the data for nuclear interactions in the telescope as well as absorption and production in the overlying atmosphere. The material in the charge-energy module to the midpoint of S2 is 8.7 g cm^{-2}. The correction to the top of the telescope takes into account the distribution of this matter and the efficiency of 90% for detecting nuclear interactions in the telescope. The further extrapolation to the top of the atmosphere uses a slab model in which the latest semiempirical cross sections for proton-nucleus interactions are adjusted to air-nucleus cross sections using the target factors presented by Westfall *et al.* (1979). Errors of ±10% are assumed for these cross sections and incorporated into the errors shown.

In Table 1 we show the intensities obtained at the top of the atmosphere and the charge abundance ratios relative to Si.

IV. RESULTS AND COMPARISON WITH OTHER DATA

The relative abundances from this experiment are compared with those from other experiments with a comparable statistical accuracy at lower energies (Garcia-Munoz and Simpson 1979: 70–400 MeV per nucleon) and higher energies (Dwyer and Meyer 1981: 1.2–2.4 GeV per nucleon) in Figure 4. The general agreement between the measured relative abundances is good although variations outside of the quoted errors, which are mainly statistical, are observed. Some energy-dependent variations would be expected from galactic propagation effects, but we believe that an important source of part of the existing differences in the balloon data could be contained in the corrections to the top of the atmosphere. To give the reader an appreciation for

TABLE 1

INTENSITIES OF VARIOUS CHARGES

Charge	C/C_m[a] (600–1000 MeV per nucleon)	Observed Events	Intensity at Top[b]	Ratio to Si
He	0.514–0.758	24,260	54.08 ± 1.1	270.3 ± 5.8
C	0.450–0.714	19,950	1.52 ± 0.03	7.60 ± 0.16
N	0.434–0.710	5,696	0.42 ± 0.01	2.08 ± 0.05
O	0.416–0.605	16,083	1.41 ± 0.03	7.07 ± 0.15
Ne	0.372–0.696	2,646	0.228 ± 0.005	1.13 ± 0.03
Na	0.361–0.693	674	0.051 ± 0.002	0.258 ± 0.011
Mg	0.326–0.685	3,228	0.282 ± 0.006	1.42 ± 0.04
Al	0.310–0.682	708	0.056 ± 0.002	0.282 ± 0.012
Si	0.264–0.675	2,260	0.202 ± 0.004	1.00
S	0.190–0.665	512	0.0467 ± 0.0019	0.231 ± 0.011
Ar	0.141–0.658	225	0.0205 ± 0.0012	0.102 ± 0.007
Ca	0.072–0.640	322	0.0323 ± 0.0015	0.161 ± 0.009
Cr[c]	... –0.624	242	0.0240 ± 0.0015	0.118 ± 0.008
Fe[c]	... –0.606	1,205	0.142 ± 0.004	0.698 ± 0.020
Ni[c]	... –0.590	61	0.0074 ± 0.0009	0.035 ± 0.005

[a] C/C_m and energy intervals are at the top of the atmosphere.
[b] In particles m^{-2} sr^{-1} s^{-1}. Mount Washington neutron monitor intensity at time of ballon flight (1977 September 1–3) = 2336.
[c] Events below Cerenkov threshold are obtained assuming a similar spectrum to Si nuclei.

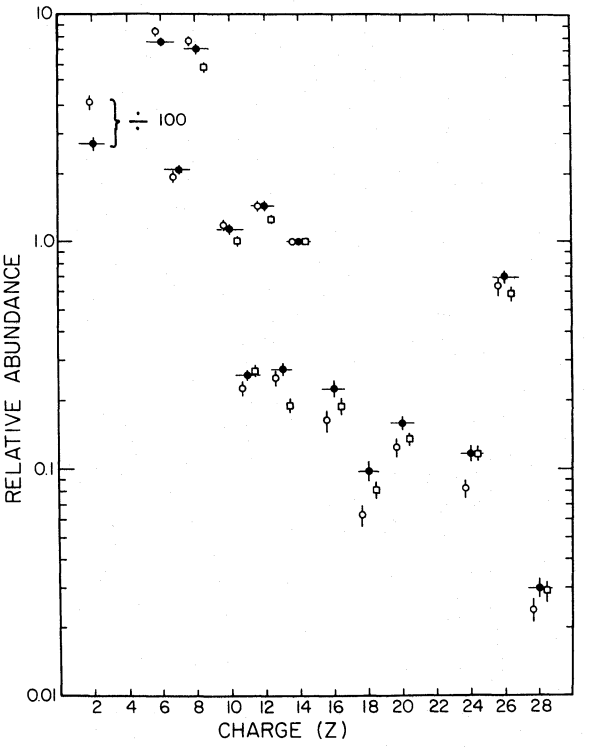

FIG. 4.—Relative abundances at the top of the atmosphere at low energies (Garcia-Munoz and Simpson 1979) (*open circle*), intermediate energies (this experiment) (*filled circle*), and high energies (Dwyer and Meyer 1981) (*open square*) for elements whose source abundances are determined in this paper.

the measurement uncertainties, we show in Table 2 the results of several measurements of the important Si/Fe ratio at ~1 GeV per nucleon. Even though all measurements lie within $\pm 3\ \sigma$ of the weighted average, there is still a significant variation in the data—one that becomes important when the energy dependence of the Si/Fe ratio is examined. Our value for this ratio is $\sim 2\ \sigma$ below the weighted average, and this difference is not large enough to alter significantly the derived cosmic-ray source abundances as long as this determination is restricted to one energy level.

TABLE 2

MEASUREMENTS OF THE Si/Fe RATIO AT ~1 GeV PER NUCLEON

Reference	Ratio
This work	1.43 ± 0.05
Lezniak and Webber 1978	1.54 ± 0.08
Young *et al.* 1981	1.77 ± 0.09
Scarlett, Freier, and Waddington 1978	1.28 ± 0.06
Fisher *et al.* 1976	1.52 ± 0.08
Israel *et al.* 1979	1.57 ± 0.10
Lund *et al.* 1975	1.66 ± 0.07
Garcia-Munoz *et al.* 1975	1.40 ± 0.10
Garcia-Munoz and Simpson 1979	1.48 ± 0.08[a]
Dwyer and Meyer 1981	1.71 ± 0.05[a]
Weighted average	1.53

[a] Adjusted to 1 GeV per nucleon assuming identical Si and Fe source spectra.

V. EXTRAPOLATION OF THE RELATIVE ABUNDANCES TO THE COSMIC-RAY SOURCE

We have derived the cosmic-ray source composition from the data obtained at Earth using an interstellar propagation model, taking into account the effects of solar modulation with $\phi = 400$ MV. A standard leaky-box model (exponential path length distribution) is assumed for galactic propagation. Ionization energy loss, secondary and higher order fragmentation, and radioactive decay are taken into account in the computer program. The fragmentation cross sections we use are the most recent semiempirical cross sections of Tsao and Silberberg (1979), modified by experimental values where available. Errors of $\pm 10\%$ for these cross sections are assumed. We extrapolated back to the source allowing the escape mean free path λ_{esc} to be a variable. Calculations were also made with a path length distribution truncated at short path lengths.

There is some evidence that not all interstellar propagation calculations, even those using the same model and same fragmentation cross sections, give the same results on the production and growth of the various charges (Freier 1980). Our calculations agree very closely with those of Stone and Wiedenbeck (1979), Simon (1977), and Shapiro and Silberberg (1975), where comparisons can be made. Significant differences exist in some cases between our calculations and the calculations performed by the Chicago group (e.g., Garcia-Munoz and Simpson 1979). These authors have noted some of these differences and suggest that they are due to the truncated path length distribution they used. As we will show shortly, however, a truncated path length distribution makes only a small effect as do other deviations from the standard leaky-box (exponential path length distribution) model.

In order to illustrate the effects of the interstellar propagation on the measured charge abundances more clearly, we shall describe them in terms of source factors—the factors needed to multiply the observed relative abundances at Earth to obtain the source abundances. The source factors presented in Table 3 are for an energy of 800 MeV per nucleon referenced to a source factor of 1.0 for Si (see also Figure 5). The source factor $S(Z, E)$ may be considered to be made up of two dominant terms

$$S(Z, E) = P(Z, E) \cdot f(Z, E) ,$$

where $P(Z, E)$ may be called the propagation factor and $f(Z, E)$ is a fragmentation factor to take care of secondary production. Thus, to obtain the source abundance j_s from the abundance observed at Earth j_e, one writes

$$j_s = j_e \cdot S(Z, E) .$$

The propagation factor for a leaky-box model is essentially

$$P(Z, E) = \left[\frac{1}{\lambda_i} + \frac{1}{\lambda_{esc}}\right] \times \Delta E ,$$

TABLE 3

EXTRAPOLATION TO THE COSMIC-RAY SOURCE FOR $\lambda_{esc} = 6 \pm 1$ g cm^{-2}

Charge	Ratio to Si	Source Factor	Source Ratio to Si	Solar Cosmic Rays
He	270.3 ± 5.8	0.44 ± 0.03	118 ± 8	416 ± 20
C	7.60 ± 0.16	0.62 ± 0.03	4.71 ± 0.22	2.74 ± 0.29
N	2.08 ± 0.05	0.13 ± 0.04	0.27 ± 0.08	0.70 ± 0.08
O	7.07 ± 0.15	0.76 ± 0.02	5.37 ± 0.19	5.80 ± 0.60
Ne	1.13 ± 0.03	0.57 ± 0.03	0.64 ± 0.03	0.97 ± 0.07
Na	0.258 ± 0.011	0.35 ± 0.06	0.090 ± 0.016	0.07 ± 0.03
Mg	1.42 ± 0.04	0.79 ± 0.02	1.12 ± 0.04	1.20 ± 0.18
Al	0.276 ± 0.012	0.54 ± 0.06	0.146 ± 0.017	0.10 ± 0.02
Si	1.00	1.00	1.00	1.00
S	0.231 ± 0.011	0.73 ± 0.04	0.168 ± 0.011	0.20 ± 0.04
Ar	0.102 ± 0.007	0.24 ± 0.06	0.025 ± 0.007	0.03 ± 0.01
Ca	0.161 ± 0.009	0.52 ± 0.05	0.083 ± 0.009	0.10 ± 0.02
Cr	0.118 ± 0.008	0.21 ± 0.09	0.025 ± 0.011	0.02 ± 0.01
Fe	0.698 ± 0.020	1.50 ± 0.06	1.04 ± 0.04	1.09 ± 0.18
Ni	0.035 ± 0.004	1.57 ± 0.06	0.058 ± 0.007	0.06 ± 0.015

where λ_i is the interaction mean free path of the ith species in hydrogen and ΔE is an energy loss term that must be computed numerically and is only weakly charge dependent in the energy range being considered here. The propagation factor will change slowly with charge mainly because of a variation in λ_i. It will be the dominant term in the source factor for charges where the secondary production is small.

The other term, the fragmentation factor, depends on the fragmentation cross sections into the species in question and the fraction of that species that can be attributed to secondary production. Schematically,

$$f(Z, E) \equiv (1 - f_{prod}/f_e) ,$$

where f_{prod} is the total secondary production of a particular charge and f_e is the observed abundance of that charge at Earth. This term has the effect of reducing the source factor and, for species for which the secondary production is dominant, leads to small source factors. In these cases, the source abundance errors are due mainly to uncertainties in the fragmentation cross sections and the escape length, λ_{esc}, which enter into f_{prod}.

Several points are worth noting with this method of presentation. First of all, because we are dealing with a single energy interval, the fact that λ_{esc} is a function of energy has very little influence on the results. Models in which the path length distribution is truncated at small path lengths effect mainly the propagation term. Examples of a 4 g cm^{-2} exponential distribution truncated with a linear rise below 1 g cm^{-2} and simple

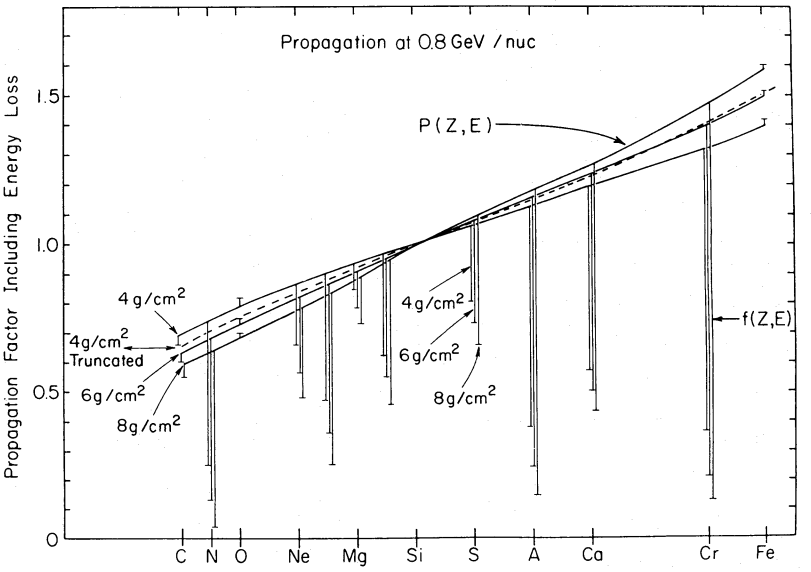

FIG. 5.—Source factors for various nuclei relative to Si. The factor $P(Z, E)$ is shown separately for various values of the escape length. This factor is multiplied by $f(Z, E)$ for these escape lengths to give the overall propagation factor as illustrated for S nuclei.

exponential path length distributions of 4, 6, and 8 g cm^{-2} of hydrogen are shown in Figure 5 which illustrates schematically how the overall source factors are obtained for several charges. Basically, the differences between truncated and exponential path length distributions become important only when comparing charges widely separated in Z.

In selecting charges for which to derive a source abundance, we have chosen only ones in which the fraction $f_{\rm prod}/f_e < 0.85$ for a nominal escape length of 6 g cm^{-2}. For other charges, the errors in the cross sections and in $\lambda_{\rm esc}$ are too large to allow meaningful source abundances to be obtained. The final source abundances that we obtain are shown in Table 3. They are based on data with a much greater statistical accuracy and better charge resolution than those derived earlier by LW, but they agree generally within $\pm 10\%$–20% with those earlier abundances and include a more precise abundance for Na, and also source abundances for Ar and Cr nuclei. An important ratio from this work is the He/O ratio which is 21.5 ± 1.5.

It should be noted that, for comparison purposes, it is frequently necessary to compare isotopic ratios of certain elements. Since isotopic abundance differences are observed between the cosmic-ray source and solar system material for Ne, Mg, Si, and possibly C nuclei (Wiedenbeck and Greiner 1981; Webber 1982), the isotopic ratios for these charges may be significantly different than the overall charge ratios. This is most important for the ratios involving the Ne isotopes where it is found that the ^{22}Ne/^{20}Ne ratio is ~ 4 times the solar ratio and the isotope ^{20}Ne is underabundant by a factor ~ 0.5 relative to solar. Examples of differences in charge and isotopic ratios of key elements involving Ne are given in Table 4 (isotope ratios after Webber 1982).

TABLE 4

COMPARISON OF CHARGE AND ISOTOPE RATIOS FOR SEVERAL CHARGES

Ratios	GCRS	SCR
Charge ratio:		
C/O	0.88	0.46
O/Ne	8.39	6.11
Ne/Mg	0.57	0.81
Ne/Si	0.64	0.97
Isotope Ratio:		
^{12}C/^{16}O	0.85	0.47
^{16}O/^{20}Ne	12.2	6.73
^{20}Ne/^{24}Mg	0.51	0.92
^{20}Ne/^{28}Si	0.46	0.89

VI. SOLAR COSMIC-RAY ABUNDANCES

Recently, the precision of solar cosmic-ray abundance measurements has improved dramatically (McGuire, von Rosenvinge, and McDonald 1979; Cook, Stone, and Vogt 1980). At the same time, our understanding of the energy dependence of the charge ratios that are observed for these particles is more complete. For energies above a few MeV per nucleon, these ratios are observed to vary about an average ratio from event to event so that, if an average ratio for many events is taken, this is believed to represent closely the average abundances for the accelerated solar material. Such an average is shown in Table 3 based on the work of Cook *et al.* It should be cautioned, however, that the cause for these variations about the average is not yet fully understood so that the use of average solar particle abundances might still be subject to systematic uncertainties.

VII. COMPARISON OF GALACTIC AND SOLAR COSMIC-RAY ABUNDANCES

If the ratio of cosmic-ray source to solar cosmic-ray abundances is formed from this data, the picture illustrated by Figure 6 emerges. Of the 15 charges compared, 11 have ratios consistent with 1 (similar abundances). This rather strong similarity was first pointed out by Webber (1975) and more recently by Cook, Stone, and Vogt (1980) and others based on improved solar cosmic-ray data. The four elements whose abundances differ significantly in the two sources are He, C, N, and Ne.

In Figure 7 the abundance ratios of galactic cosmic-ray sources to solar cosmic rays (GCRS/SCR) are plotted versus first ionization potential. Here a very weak correlation, if any, is seen to exist, although it could be argued that those elements with the highest ionization potential are underabundant in the galactic cosmic-ray

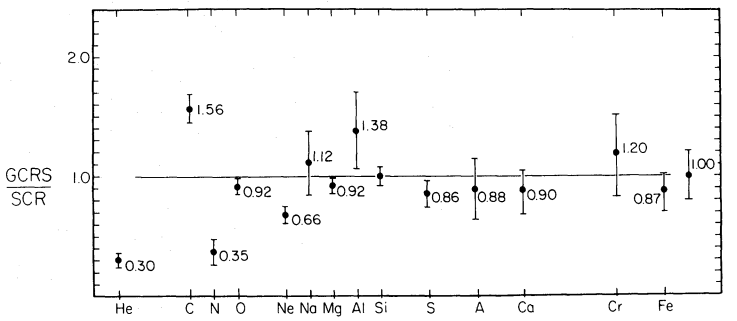

FIG. 6.—Ratio of charge abundances, GCRS to SCR

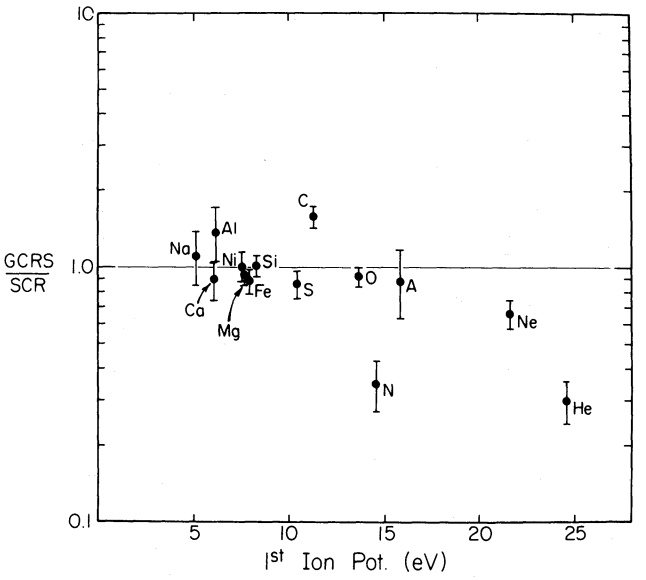

FIG. 7.—Ratio of charge abundances, GCRS to SCR, vs. first ionization potential.

source. It is also possible to conclude that another type of selective effect influencing only the relative abundance of He, C, N, and Ne is at work, and that it is not necessarily related to first ionization potential. We shall return to this discussion after we have presented various nonaccelerated abundance compilations and compared them with the cosmic-ray abundances.

VIII. ABUNDANCE COMPILATIONS FOR SOLAR SYSTEM MATERIAL

We compare the abundances of accelerated particles with several types of other abundance compilations as illustrated in Table 5, including the following:

TABLE 5

COMPARISON OF VARIOUS ABUNDANCE COMPILATIONS

Charge	SS[a]	LG[b]	Photosphere[c]	Corona[d]
He	1800	2700	1410	Uncertain
C	11.1	13.0	9.33	11.35
N	2.31	2.30	1.95	1.07
O	18.4	23.0	15.5	6.30
Ne	2.60	2.70	0.83	1.00
Na	0.06	0.056	0.043	0.071
Mg	1.06	1.05	0.89	1.00
Al	0.085	0.084	0.074	0.074
Si	1.00	1.00	1.00	1.00
S	0.50	0.45	0.35	0.33
Ar	0.106	0.09	0.022	Uncertain
Ca	0.063	0.062	0.05	Uncertain
Cr	0.013	0.013	0.0115	Uncertain
Fe	0.90	0.88	0.71	1.00
Ni	0.048	0.048	0.043	0.051

[a] Cameron 1980.
[b] Meyer 1979.
[c] Ross and Aller 1976.
[d] Parkinson 1977; Mariska 1980.

1. Solar system abundances after Cameron (1980). These are the most common abundances used to compare with both galactic or solar cosmic rays. Generally, the Cameron abundances are derived from C1 type meteorites. However, the C, N, and O abundances are normalized to Si from the solar photospheric data of Ross and Aller (1976). Also, the abundances of He, Ne, and Ar are obtained by extrapolation, or, in some cases by using (earlier) solar cosmic-ray abundance data.

2. Local galactic abundances after Meyer (1979). A variety of abundance data is used in this compilation. The abundances here do not differ significantly from those of Cameron for the charges we are interested in. Thus, the first and second compilations are interchangeable in spite of their somewhat different data base.

3. Solar photospheric abundances after Ross and Aller (1976). These abundances are all derived principally from solar photospheric measurements with the exception of Ne and Ar which are derived from (earlier) solar cosmic-ray measurements. These two elemental abundances differ significantly in this compilation from those of the first and second compilations because of a different normalization procedure. There are also differences in the relative He, C, N, and O abundances.

4. Solar coronal abundances. Here, we have used a combination of several recent measurements (Parkinson 1977; Mariska 1980) that seem to reach a consensus on a much lower O/Si ratio than exists in the first, second, or third compilations. The differing O/Si ratio obtained from photospheric and coronal measurements is discussed by Parkinson, but it is not yet clear whether this represents a real composition difference between these two locations. Suffice to say that these differences will be very important when comparing these abundances with galactic or solar cosmic rays.

IX. ABUNDANCE COMPARISONS

If a traditional comparison between the galactic cosmic-ray abundances and local galactic abundances is made using first ionization potential as a parameter, the results depicted in Figure 8 are seen. A correlation with first ionization potential is obvious, although there are significant variations beyond a strict one-to-one correlation. Note that the same correlation will appear for the GCRS/SS ratio, since the solar system (SS) abundances are virtually identical to the local galactic ones. There is some tendency for the data to be grouped into two classes—those elements with ionization potential less than and those with ionization potential greater than ~ 10 eV. It should be noted, however, that the elements with $I > 10$ eV include C, N, O, and He, Ne, and Ar, all of whose abundances are obtained by a different set of procedures than used for the other elements in the local abundance compilations.

Next we compare the solar cosmic-ray abundances with the solar system abundances using first ionization potential as a parameter in Figure 9. Any differences between this correlation and that in Figure 8 must be due to differences in galactic and solar cosmic-ray composition since the data base comparison is essentially the

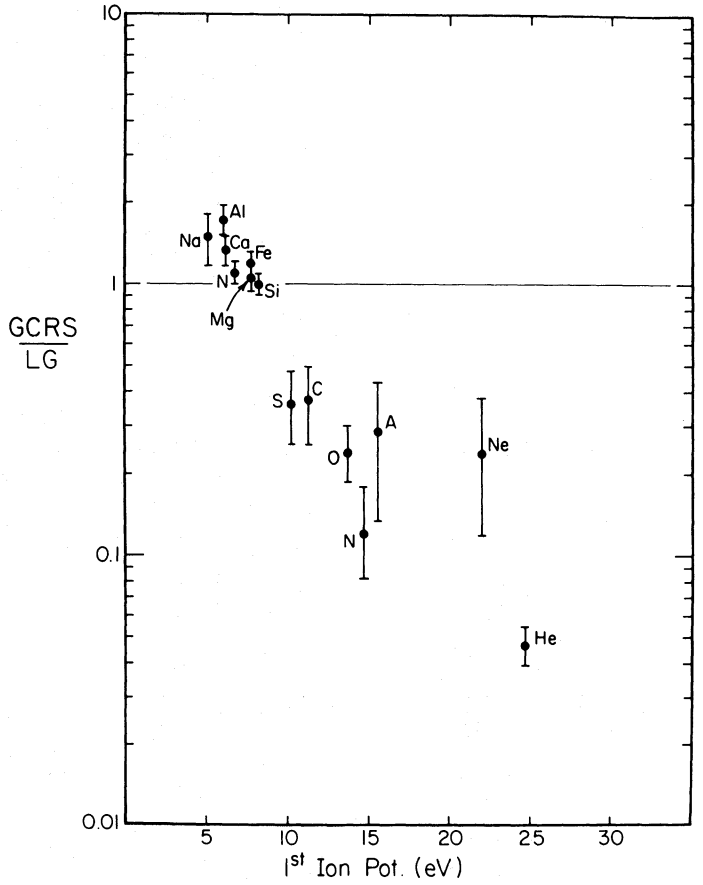

FIG. 8.—Ratio of charge abundances, GCRS to local galactic material, vs. first ionization potential

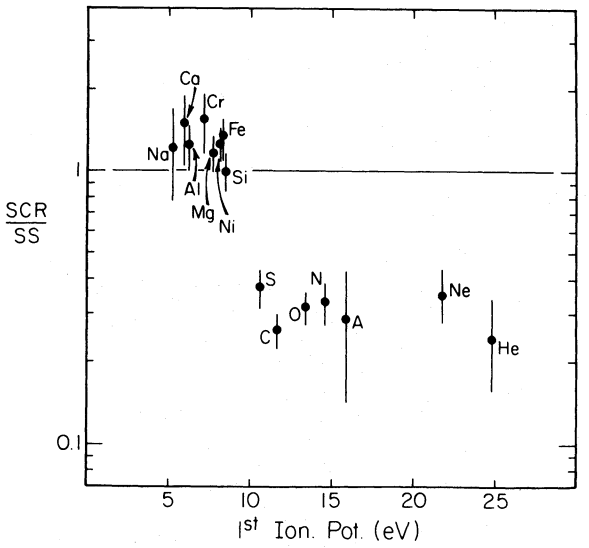

FIG. 9.—Ratio of charge abundances, SCR to solar system abundances, vs. first ionization potential.

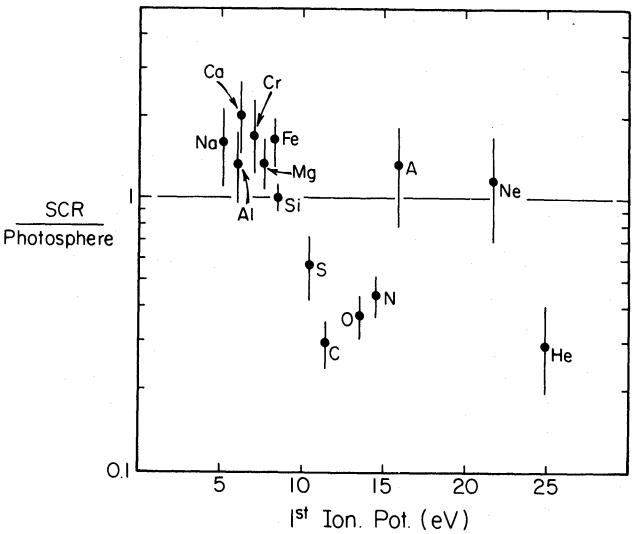

FIG. 10.—Ratio of charge abundances, SCR to photospheric abundances, vs. first ionization potential.

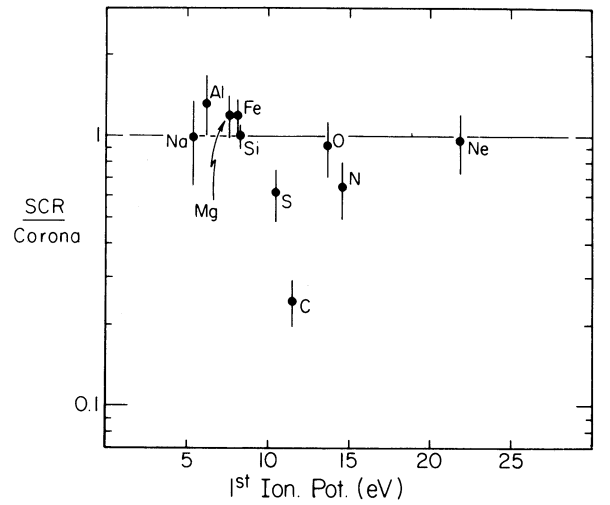

FIG. 11.—Ratio of charge abundances, SCR to coronal abundances, vs. first ionization potential.

same. Here the separation into two classes of elements at an ionization potential $\sim$ 10 eV is even more striking.

It would be more useful, however, to compare the solar cosmic-ray abundances directly with the abundance of material in the acceleration regions themselves which are presumably in the solar corona. As a first step to this kind of comparison, the solar cosmic-ray abundances are compared with photospheric abundances in Figure 10, again using first ionization potential as a parameter. Here, the correlation with first ionization potential and the discontinuity in abundance ratios at $\sim$ 10 eV, is much less convincing. This is due mainly to the different He, Ne, and Ar abundances used in the photospheric compilation. The abundances of these elements are derived from solar cosmic rays in each case but using different normalization procedures!

And, finally, the most direct comparison of all, between solar cosmic rays and solar coronal abundances is made in Figure 11. Here, there is no correlation with first ionization potential at all, and, in fact, except for C, the two species have generally the same abundance. If this comparison is accepted at face value, then the evidence for preferential acceleration effects for solar cosmic rays is very limited, and the abundance differences between solar cosmic rays and other solar abundance compilations are due mainly to an abundance difference in the corona itself. Several possible suggestions have been made for producing abundance differences between the photosphere and the corona, as noted by Mariska (1980). It seems that the key to understanding this problem is the O/Si ratio in the various abundance compilations. In addition to the C and N abundances which are usually referenced to O, the abundances of the elements He, Ne, and Ar, as obtained from solar cosmic rays, depend critically on whether the normalization is made with respect to O or to Si. Until these problems are cleared up, it is difficult to support the idea of a preferential acceleration effect as being responsible for the dominant first ionization potential effects seen in Figures 8 and 9.

It should be remarked here that there is indeed strong evidence for certain types of preferential acceleration in the solar cosmic rays. This is indicated by the unusual ^{3}He abundances observed in several events and also by abundance variations about the average as observed from flare to flare (e.g., Fe-rich flares) (Cook, Stone, and Vogt 1980). These effects may be related to various plasma processes on the Sun, and a very likely model is the one proposed by Fisk (1978), in which the ion cyclotron waves resonantly heat ^{3}He and certain ions of heavier elements with a similar mass-to-charge ratio to a far greater temperature than ions with $A/Z_{\rm eff} = 2.0$, such as ^{4}He and ^{12}C. This process could be responsible in part for the abundance differences noted in Figures 8 and 9. Other possible models that explain differences in solar cosmic-ray and solar system material via preferential acceleration processes have been advanced by Cassé and Goret (1978) and by Mullan and Lavine (1981). Both of these models are two-stage models; the first stage involves first ionization potential and the second stage requires an injection process depending on magnetic rigidity. Before either of these models is required to explain *all* of these differences, however, one needs to resolve the O/Si ratio dilemma and to verify whether the elemental selection is taking place between the photosphere and the corona or between the corona itself and the solar cosmic rays.

Meanwhile, abundance differences between two samples of accelerated matter, galactic and solar cosmic rays, clearly do exist. If preferential acceleration is assumed to occur in both sources, then it must be operating in a different manner to produce the abundance differences. Or, alternatively, the source material itself must have different abundances. The abundance differences between galactic and solar cosmic rays are rather selective, and it seems worthwhile to examine whether they could be the result of abundance differences in the two sources, i.e., basically the result of different nucleosynthesis histories. This point of view receives considerable support from recent measurements which indicate that the abundance of ^{22}Ne and possibly the heavy isotopes of Mg and Si as well are enhanced in the cosmic-ray source relative to solar abundances (e.g., Wiedenbeck and Greiner 1981). A possible explanation for these particular enhancements has already been suggested by Woosley and Weaver (1981); see also Arnett 1969). Their supermetallicity model predicts approximately equal enhancements of ^{22}Ne, ^{26}Mg, and ^{30}Si, as well as a variety of other neutron-rich isotopes. In this model, for regions enriched in metals, He burning accompanied by the reaction sequence

$$^{14}\mathrm{N}(\alpha, \gamma)^{18}\mathrm{F}(\beta^+, \nu)^{18}\mathrm{O}(\alpha, \gamma)^{22}\mathrm{Ne}$$

results in increases in the heavy isotopes, such as ^{18}O, ^{22}Ne, ^{26}Mg, ^{30}Si, etc. Further reactions convert part of this excess into free neutrons which then react with heavy nuclei to produce other enhancements of neutron-rich isotopes. Overall, in this process, the additional processing of both ^{4}He and ^{14}N may result in an underabundance of these elements in the cosmic-ray source relative to the solar source *as indeed is observed*. Quantitative

calculations of the underabundance of these elements is expected to be difficult because of the possible dilution of this stellar material with the interstellar gas at the cosmic-ray source.

The other elements in the cosmic-ray source with different relative abundances are C and Ne, or more specifically ^{12}C and ^{20}Ne. The abundances of these elements are connected in the nucleosynthesis cycle through explosive C burning following the He burning that produces the initial ^{12}C and ^{16}O abundances. A wide variety of senarios are possible for the C burning (e.g., Pardo, Counch, and Arnett 1974). Most of these senarios start out with $^{12}C/^{16}O \lesssim 1$, and, throughout the C burning, this ratio becomes even less, e.g., it is generally adjusted to fit the solar ratio of 0.46. To obtain a larger $^{12}C/^{16}O$ ratio, it is required that the initial ratio be larger, a function of the He burning (which is apparently still uncertain [Arnett 1977]), or that the C burning be incomplete (e.g., at a lower temperature than usually assumed), or that both of these conditions occur. A lower temperature burn will result in a lower ^{20}Ne abundance as is seen in the cosmic-ray source. This will also modify the abundances of the isotopes of Na, Mg, Al, and Si; in particular, a low ^{24}Mn abundance should also be expected, and this is not the case.

The new abundance ratios presented here, along with the observed isotopic abundance differences, present a challenge to nucleosynthesis theory, as well as to preferential acceleration models, and until more detailed calculations are made in both areas, it does not seem possible to understand completely these galactic and solar cosmic-ray abundance differences.

Another perspective on the galactic cosmic-ray relative abundance measurements can be obtained by a comparison with recent, interstellar material abundance measurements, particularly those from supernova remnants which are considered to be prime regions for the origin of the cosmic rays. The particular abundance variations observed for a Type I remnant (Cas A) (Becker *et al.* 1980) or a Type II remnant (Puppis A) (Canizares and Winckler 1981) do not correlate in any way with the observed cosmic-ray source abundance for the several elements where the comparison can be made.

There is evidence that the interstellar medium may be enriched in ^{13}C relative to ^{12}C by a factor ~ 2 relative to solar abundances (Wannier 1980), and this type of enrichment may also exist in the cosmic-ray source abundances. However, other patterns of abundance similarities between these two classes of material involving both charges and isotopes have not been established.

X. SUMMARY AND CONCLUSIONS

The relative charge abundance of galactic cosmic-ray nuclei has been measured between 600–1000 MeV per nucleon over a wide range of Z from 2–28. The abundances observed at Earth have been extrapolated to the cosmic-ray source yielding accurate source abundances for 15 nuclei. These abundances, along with isotopic abundances ratios obtained in the same experiment (Webber 1982) and by Wiedenbeck and Greiner (1981), are compared with the average abundances observed in another sample of accelerated material–solar cosmic rays. Significant differences are found in the composition for the elements He, C, N, and Ne. For Ne, the $^{22}Ne/^{20}Ne$ ratio is ~ 4 times greater in the cosmic-ray source than in solar cosmic rays, which, coupled with the low abundance of Ne, means that ^{20}Ne in galactic cosmic rays is underabundant relative to solar cosmic rays by a factor ~ 2. These galactic and solar cosmic-ray abundances are compared with those of a variety of samples of unaccelerated matter. The usual correlations with first ionization potential are observed when the comparison is with "solar system" abundance compilations. However, possible normalization problems for the O/Si ratio and for various abundances such as He, Ne, and Ar, which are obtained from solar cosmic-ray measurements in the first place, are found in many of the nonaccelerated abundance compilations. These are such that they may completely wash out solar cosmic-ray and solar abundance differences, and indeed there is little evidence of any difference between the most recent coronal abundance data and solar cosmic rays.

In view of these difficulties, we have examined more carefully the very clear differences apparent in the two accelerated species, galactic and solar cosmic rays. At the present time, these differences seem to be explained more easily in terms of different nucleosynthesis histories rather than preferential acceleration effects. In particular, one explanation of enhanced ^{22}Ne and other heavy isotopes in galactic cosmic rays is ^{4}He burning in metal-rich regions via a reaction sequence involving ^{14}N. Additional processing of ^{4}He and ^{14}N might explain both the underabundances of these isotopes and the overabundance of isotopes such as ^{22}Ne and ^{26}Mg in the cosmic-ray source. It is further noted that the ^{12}C overabundance and ^{20}Ne underabundance in the cosmic-ray source may be related to details of the He-burning process followed by explosive C burning.

The new cosmic-ray source charge ratios presented here, along with specific isotopic abundance differences that are observed, require new calculations in the areas of both nucleosynthesis theory and preferential acceleration and present a new challenge to the attempt to locate the source regions of galactic cosmic rays.

This work was supported under NASA grant NGR-30-002-052. Many people were responsible for the construction of the instrument, balloon flight, and data analysis used here. I particularly want to acknowledge the efforts of Jim Kish and Dr. Jerry Lezniak in various phases of this work.

REFERENCES

Arnett, W. D. 1969, *Ap. J.*, **166**, 153.
———. 1977, Preprint 77–26, Enrico Fermi Institute, Chicago.
Becker, R. H., Holt, S. S., Smith, B. W., White, N. E., Bolt, E. A., Mushotzky, R. F., and Serlemitsos, P. J. 1980, *Ap. J.* (*Letters*), **235**, L5.
Binns, W. R., Fickle, R. K., Garrard, T. L., Israel, M. H., Klarmann, J., Stone, E. C., and Waddington, C. J. 1981, *Ap. J.* (*Letters*), **247**, L164.
Cameron, A. G. W. 1980, Preprint 1357, Harvard-Smithsonian Center for Astrophysics, Cambridge, Massachusetts.
Canizares, C. R., and Winckler, P. F. 1981, *Ap. J.* (*Letters*), **246**, L33.
Cassé, M., and Goret, P. 1978, *Ap. J.*, **221**, 703.
Cook, W. R., Stone, E. C., and Vogt, R. E. 1980, *Ap. J.* (*Letters*), **238**, L97.
Dwyer, R., and Meyer, P. 1981, *Proc. 17th Int. Cosmic Ray Conf.* (Paris), **2**, 54.
Fisher, A. J., Hagen, F. A., Maehl, R. C., Ormes, J. F., and Arens, J. F. 1976, *Ap. J.*, **205**, 938.
Fisk, L. A. 1978, *Ap. J.*, **224**, 1048.
Freier, P. S. 1980, Paper presented at A.P.S. Meeting, September 3–6, Minneapolis, Minnesota.
Garcia-Munoz, M., Juliusson, E., Mason, G. M., Meyer, P., and Simpson, J. A. 1975, *Ap. J.*, **197**, 489.
Garcia-Munoz, M., and Simpson, J. A. 1979, *Proc. 16th Int. Cosmic Ray Conf.* (Kyoto), **1**, 270.
Havnes, O. 1973, *Astr. Ap.*, **24**, 435.
Israel, M. H., Klarmann, J., Love, P. L., and Tueller, J. 1979, *Proc. 16th Int. Cosmic Ray Conf.* (Kyoto), **1**, 323.
Kristiansson, K. 1971, *Ap. Space Sci.*, **14**, 485.
Lezniak, J. A. 1975, *Nucl. Instr. Meth.*, **126**, 129.
Lezniak, J. A., and Webber, W. R. 1978, *Ap. J.*, **233**, 676 (LW).
Lund, N., Rasmussen, I. L., Peters, B., Rotenberg, M., and Westergaard, N. J. 1975, *Proc. 14th Int. Cosmic Ray Conf.* (Munich), **1**, 263.
Mariska, J. T. 1980, *Ap. J.*, **235**, 268.
McGuire, R. E., von Rosenvinge, T. T., and McDonald, F. B. 1979, *Proc. 16th Int. Cosmic Ray Conf.* (Kyoto), **5**, 61.
Meyer, J. P. 1979, *Proc. 16th Int. Cosmic Ray Conf.* (Kyoto), **2**, 115.
Mullan, D. J., and Levine, R. H. 1981, *Ap. J. Suppl.*, **47**, 87.
Pardo, R. C., Counch, R. G., and Arnett, W. D. 1974, *Ap. J.*, **191**, 711.
Parkinson, J. H. 1977, *Astr. Ap.*, **57**, 185.
Ross, J. E., and Aller, L. H. 1976, *Science*, **191**, 1223.
Scarlett, W. R., Freier, P. S., and Waddington, C. J. 1978, *Ap. Space Sci.*, **59**, 301.
Shapiro, M. M., and Silberberg, R. 1975, *Phil. Trans. Roy. Soc. London*, A. **277**, 317.
Simon, M. 1977, *Proc. 15th Int. Cosmic Ray Conf.* (Plovdiv), **2**, 125.
Stone, E. C., and Wiedenbeck, M. E. 1979, *Ap. J.*, **231**, 606.
Tsao, C. H., and Silberberg, R. 1979, *Proc. 16th Int. Cosmic Ray Conf.* (Kyoto), **2**, 202.
Wannier, P. G. 1980, *Ann. Rev. Astr. Ap.*, **18**, 399.
Webber, W. R. 1975, *Proc. 14th Int. Cosmic Ray Conf.* (Munich), **5**, 1597.
———. 1982, *Ap. J.*, **252**, 386.
Westfall, G. D., Wilson, L. W., Lindstrom, P. J., Crawford, A. J., Greiner, D. E., and Heckman, H. H. 1979, *Phys. Rev. C*, **19**, 1309.
Wiendenbeck, M. E., and Greiner, D. W. 1981, *Proc. 17th Int. Cosmic Ray Conf.* (Paris), **2**, 76.
Woosley, S. E., and Weaver, T. A. 1981, *Ap. J.*, **243**, 651.
Young, J. S., Freier, P. S., Waddington, C. J., Brewster, N. R., and Fickle, R. K. 1981, *Ap. J.*, **246**, 1014.

W. R. WEBBER: Space Science Center, University of New Hampshire, Durham, NH 03824